

Microstructural Study & Assessment of Endurance Limit Through Numerical Simulation in TIG welded Aluminum Alloy (AA2219-T87)

M. Ullah¹, G. Y. Chohan², Q. Ali³, M. A. Nasir⁴

¹*School of Material Science & Engineering, Shandong University, P. R. China*

^{2,3}*Department of Mechanical Engineering, UCET, University of Sargodha, Pakistan*

⁴*Department of Mechanical Engineering, UET Taxila, Pakistan*

¹mudaser_me150@yahoo.com

Abstract-Tungsten Inert Gas (TIG) welding is the most common practice in aluminum alloys. It is necessary to devise a fail-safe design against fatigue failure of welded structures. Under the presence of cyclic load fatigue life is usually predicted by endurance limit of working material. In this research paper a comprehensive effort is made to investigate the endurance limit of aluminum alloy AA2219-T87. A four point rotating & bending fatigue testing machine is used to test the fatigue life estimation of the said alloy. Results obtained through experimentations are verified through numerical simulation by using software package ANSYS Workbench 14. 0. A brief microstructural study is also performed using metallurgical microscope. A gigantic contrast in grain structure is observed in different zones, formed due to TIG welding. Variation in material strength due to grains shifting from unwelded base metal (BM) to weld nugget zone (WZN) is also studied in this research.

Keywords-Fatigue Life, TIG Welding, S-N Curves, Finite Element Analysis (FEA), Microstructure

I. INTRODUCTION

In the start of nineteenth century, some engineers found that in some mechanical component failure is taken place at a stress value that was lower than the yield point [i]. It was very interesting for them that the components like shafts and bolts made of a ductile material were some time failed unexpectedly like brittle material. They observed that initially there was no flaw in workmanship of that material; however all fractured components were experiencing the fluctuating or cyclic load and this feature was common to all such cases [ii]. So such type of failure occurring at a stress lower than the yield strength in the presence of cyclic load was named as fatigue failure. Fatigue failure is the most prominent factor of failure being

studied from previous 160 years and it is happened due to the microstructural variations in the service material. In design of engineering components it is necessary to fully estimate the fatigue life [iii]. To avoid from fatigue cracking a comprehensive troubleshooting is performed before putting the model in service. The main approaches used in fatigue crack modeling are as: (1) Stress based, S-N Curve (2) Strain Based (3) Fracture Mechanics Approach [iv]. Fracture mechanics based approach is widely used in tackling the fatigue problems in metal world. It is conventional to check the fatigue life of notched specimens. It is investigated that there are two types of effects that are related to notches, statistical size effect and geometrical size effect. Statistical size effect is estimated with the maximum depth of already initiated crack in subjected material provided that the fluctuation in stresses in effective area is very high [v]. In other words it is tried to describe as when specimen is experiencing varying cyclic load then there are a large number of micro cracks are generated in its whole volume and sometimes the crack branches are created and these may totally different on both side of whole thickness [vi]. If the geometry of structure and situations of loadings are completely known then fatigue strength is calculated by fatigue-damage theory by applying S-N curves. However it is explored that this type of fatigue prediction acknowledge a little bit about the behavior of that component [vii]. After welding of the components there is aging takes place and fatigue strength lowers due to the aging of the materials. So S-N curves entertain the designer valuable information about the duration of structure as shown in Fig. 1.

The most portion of the curve is called endurance limit [viii]. Endurance limit is the boundary below which the structure bears infinite numbers of cycles without failure.

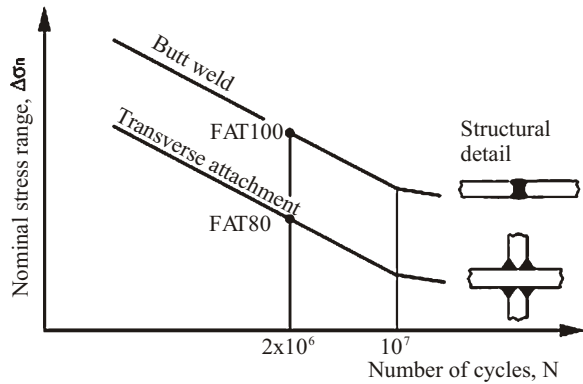


Fig. 1. S-N curves for different types of attachment of weldment

TABLE I
CHEMICAL COMPOSITION OF BASE METAL & FILLER ALLOY

Alloy	Al	Si	V	Cu	Mn	Mg	Zr	Ti	Fe	Zn
AA2219	Balance	0.2	0.04	6.3	0.3	0.02	0.18	0.06	0.23	0.04
AA2319	Balance	0.2	0.02	6.3	0.3	0.02	-	0.015	0.3	0.18

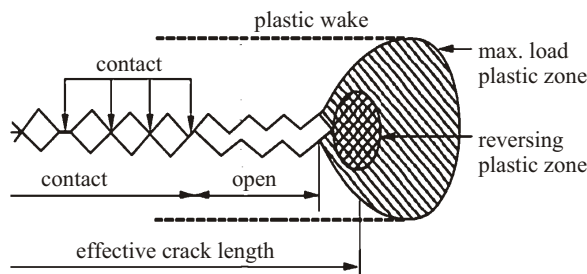


Fig. 2. Crack closure behavior [x]

A large number of researches have made attempts to understand the influence of the mean stress on the fatigue crack growth rate based on the crack closure argument. Except for high stress ratios, the fatigue crack growth can be affected more or less by the crack closure induced by plasticity in the two-parameter crack growth rate relation zone, Paris regime, or by oxidation and surface roughness. TIG welding is the most common welding in aluminum alloy [xi]. This type of welding has appreciating joint strength with respect to other types of welding especially in alloys mostly used in aerospace industry like AA2219-T87. In aeronautical structures it is the more suitable to weld the specimen rather than riveting. TIG welded aluminum alloys show lower notch sensitivity with respect to unwelded base metal. There is somehow tempering of specimens is also taken place due to welding temperature [xii]. During the TIG welding of aluminum plates it is visualize that a continuous bead structure is formed and these beads have a very drastic effect on fatigue life of specimen [xiii].

It is also concluded that there is large effect of temperature produced during TIG welding along with

However there is one limitation about these curves is that these cannot predict the fatigue life of the material for stress ratios which are other than the designed ones [ix]. However for these stress ratios which are not covered by S-N curves can be easily tackled by Goodman Diagram but these are also helpless to predict the fatigue life under various specimen's geometry, conditions of surface and special characteristic of material. Crack closure has played a central role in the study of fatigue crack propagation as shown in Fig. 2 [x].

the mixture of shielding gases on total fatigue life of the specimen. Normally for aluminum alloys the fatigue life is increased when the testing is performed on low temperature while it is decreased when shielding is increased [xiv]. Different grain refinement techniques actually define the intergranular or transgranular fatigue crack propagation. Grain boundaries concentrations also affect the fatigue crack speed [xv]. Grain boundaries with different concentration of secondary particles in aluminum alloys have different fatigue strength.

In this research paper the variation in tensile strength and hardness after TIG weldment is elaborately discussed. The calculation of fatigue strength of TIG welded AA2219-T87 is also monitored through S-N curves. All fatigue related data is also tested and verified through numerical simulation using ANSYS software. Grain structure is also studied to view the microstructural changes taken place after TIG weldment.

II. EXPERIMENTAL

A. Material

In this research AA2219 is used to study the fatigue crack propagation in base metal and TIG weld nugget zone. It is wrought aluminum alloy and due to its vast applications in aerospace industry, it is necessary to study it on experimental basis especially under cyclic loading as the most adverse factor for aerospace structures is fatigue loadings or repeating loads. The chemical composition of subjected aluminum alloy is shown in Table I.

The dominating alloying component in AA2219 is Cu. Due to high strength to weight ratio it is used

In manufacturing of cryogenic tanks. Actually the abundance of Cu in this alloy of 2XXX series furnishes the subjected alloy with aerospace desired properties. The solidus and liquidus temperature for AA2219 is noted 543°C and 643°C respectively. However the annealing temperature of research material is nearly 413°C. The mechanical properties of research materials are described in Table II.

TABLE II
MECHANICAL PROPERTIES OF AA2219

Sr. #	Property	Value
1	Hardness, Vickers	149
2	Modulus of Elasticity	73.1 GPa
3	Tensile Strength	170 MPa
4	Poison Ratio	0.33
5	Shear Modulus	27 GPa

In this research the base metal AA2219 is optimized by using pre weld heat treatment process instead of post weld heat treatment process studied and investigated by many researchers. According to ASTM [xvi] international for best aerospace properties, the performed heat treatment is designated with a code T87. The detail description of this type of heat treatment process is explained in Fig. 3.

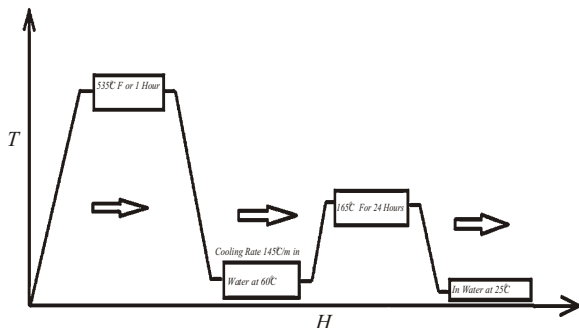


Fig. 3. Details of T87 Heat Treatment

B. Specimen Preparation

Dogbone specimens are prepared for tensile and fatigue test according to ASTM standards [xvii]. The specimens used in fatigue tests are cut from round circular bar while the specimen used in tensile test are cut from alloy sheet. The dimensions of the specimen are shown in Fig. 4.

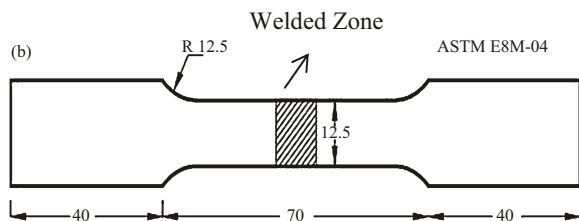


Fig. 4. Dogbone Specimen

The specimen used for fatigue tests are cut and tapered from the center and then TIG welded using AA2319 filler alloy. A V-notch of depth 1mm is grooved in the center of the welded specimen [xviii]. The welding parameters are shown in Table III.

C. Experimental procedure

Brinnell hardness tests are performed to evaluate the changes taken place after TIG welding. A series of reading from WNZ to BM is taken by using hardness tester of model HBRVU-187.5. The tensile tests are performed to find out the percentage reduction in tensile strength after TIG welding. Tensile tests are performed on a servo hydraulic universal testing machine of model MTS 810. In order to study the fatigue behavior of the notched specimens, 4 point rotating bending fatigue testing machine as shown in Fig. 5.



Fig. 5. Fatigue test experimental setup

D. Optical Microscopy

The metallography of welded specimens is performed by using Olympus DP-20 metallurgical microscope. Small pieces of welded section of weldment were cut-off and further surface preparations techniques are made to visualize the grain growth behaviors. Firstly the specimens are made scratches free by using emery paper ranging from 800 to 1200 grits. After this the specimens are creamed with universal polishing paste (Model no. UPP 841-0602) and rubbed with leather pad. Finally the specimens are polished with synthetic diamond crystal paste of grades (W-40) and (W-1.5) respectively. For AA2219 the chemical etchant according to ASM standards is Keller's reagent (5ml HNO₃ (conc.), 2ml HF (48% conc.), 3ml HCL (conc.), and 190ml distilled H₂O) [xix].

III. MODELING AND SIMULATION

After created a model in Pro/ENGINEER wildfire 5.0, IGS file of this modeling is created to open this on ANSYS software. The specimen selected for thorough finite element analysis on software package ANSYS Workbench 14.0 is 2D plane stress model. The purpose of using this software package is to achieve the objective of research easily without the interruption of

unnecessary parameters. As the specimen loading on four point rotating & bending machine is supposed to just like a beam so stress distributions are considered uniform. Stress application points are shown in Fig. 6. Linear elastic conditions are considered to just obtain the value of bending stresses which are responsible for deflection in the specimen. These numerically obtained values are then used in the formula designed for non-linear behavior of S-N curves. Non linearity consideration during the simulation will yield a value of bending stress that is incompatible with the formula generally developed for S-N curves due to overlapping effects. At such situation, a new complex calculation is advised with so many parameters which make the application of research much more difficult. So in this research, simplicity is preferred over super accurate value obtained through non-linear complex equations. And it is the core reason to use the liner elastic model instead of elastic-plastic model.

For different loading conditions ranging from 150 N to 350 N and the number of cycles at which a specific loaded specimen shows failure, the resulting stresses are found by simulations. In the conventional method of crack analysis at the notch root, the crack tip is modeled by a focused concentric ring of triangular, 3-node linear plane stress (CPS3) type elements. Around this crack tip six concentric rings of 4-node, bilinear plane stress quadrilateral elements with reduced integration (CPS4R) are modeled. The loading and boundary conditions are applied same as adopted in experimentations as shown in Fig. 6.

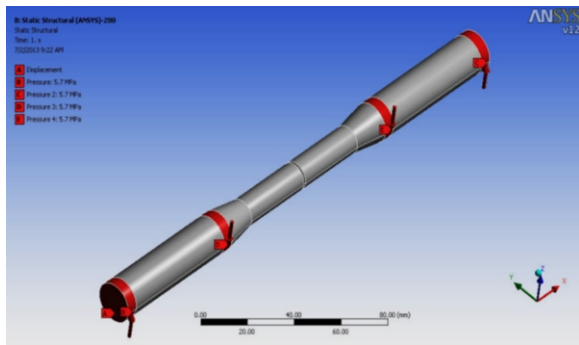


Fig. 6. Loading & Boundary conditions applied

In meshing of the elements the triangular and quadrilateral rings are concentric in the same geometry so there centre point is defined as crack front. The 2D FEA mesh consists of 950 elements and 1020 nodes. The partition line or crack path can be established by a transverse plane which extends from the specimen edge to the crack tip defined by the centre of the concentric ring mesh. During simulation, the software automatically duplicates the nodes around the crack plane, separating the two surfaces. This produces a singularity at the crack front. Small strain analysis is run to remove the errors due to presence of singularity.

The equivalent stresses produces under the action of bending and rotating loads are shown in Fig. 7.

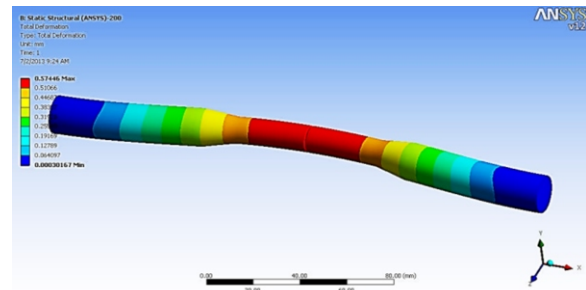


Fig. 7. Analysis of stresses in ANSYS workbench

The maximum stresses are generated at the centre of the specimen where the notch exist and crack initiation and propagation is taken place. The intensity of stresses is gradually decreases from crack front to edges of the specimens. The whole simulation is performed by considering the total linear elastic model. There are many complexities and limitations in elastic-plastic model due to specimen's geometry and combined loadings (cyclic & bending) conditions in this research simulations.

IV. RESULTS DISCUSSION

A. Tensile Test

After TIG welding it is observed that there is reduction of tensile strength is taken place up to 10-12%. The reduction in tensile strength in welded specimens is represented in Fig. 8. Actually the sudden cooling of molten metal pool at WNZ is the prime factor of tensile strength decline at the weldment. Because there is no time for the proper arrangement of grains in a sequenced manner resultantly welded material fails to establish a primary network of bonding. Thermal residual stresses are another cause of tensile strength lowering which are induced in weldment due to high temperature flame of TIG welding. Due to this cause there is also loss of ductility in weldment and welded material become more brittle.

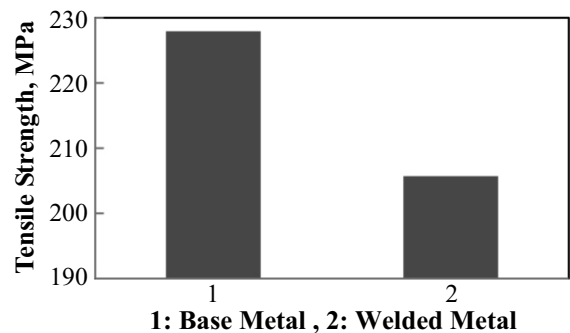


Fig. 8. Tensile strength of BM and welded specimens

B. Hardness Test

The reason of high hardness number of BM is due to presence of high amount of α -Al; however some amount is disturbed while performing pre-heat treating. The intermetallics are arranged in such a manner that they are providing the maximum strength to base metal. As it is very far away from heat source so the effects of welding temperature are very negligible on this zone. The hardness number of HAZ is greater than weld nugget zone while lower than the base metal as shown in Fig. 9. The thickness of this zone is totally varying from notch tip to the end of the specimen. In this zone the hardness number is suddenly lost due to improper recrystallization of semi-melted portion of metal. The readjustment of second phase particles in this zone is not helpful to provide proper strength to the subjected alloy. Due to high temperature, the main alloying component, Cu, is melted and move away from this zone to molten pool of weld nugget zone causing the strength decrement of this zone. WNZ is the most important area of weldment because it is the real joint portion of two bulk materials. This zone is created by a molten pool of base metal and filler alloy. It is the most fragile zone having the lowest hardness number as compared to other competitive zones. In this zone the recrystallization of molten metal pool is taken place very quickly. During rapid recrystallization of grains the strengthening particles failed to find proper positions in grain structure. In this zone some secondary particles concentrate on grain boundaries are also helpful in decreasing the hardness of the WNZ. There is dendritic structure is formed after recrystallization in this zone and as the dendritic structure depicts the softer area so resultantly this zone has lowest hardness number.

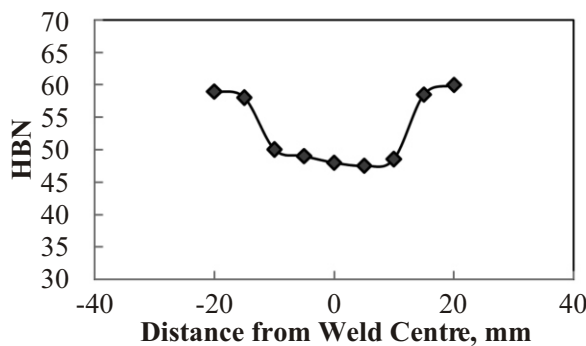


Fig. 9. Microhardness of TIG welded AA2219-T87

C. Fatigue Test

The fatigue test is performed on four point rotating and bending fatigue testing machine. The loads applied on the test specimens are converted to equivalent stresses so that the assessment of the S-N curve becomes possible. The equivalent stresses for each respective load can be calculated by using following equations

$$\frac{\sigma}{C} = \frac{M}{I} \tag{1}$$

$$\frac{\sigma}{D} = \frac{W \cdot \frac{l}{2}}{\frac{\pi}{64} \cdot D^4} \tag{2}$$

By putting the $l=110$, a general equation is achieved to convert the load into equivalent stresses

$$\sigma = \frac{W(N) \cdot 55(mm) \cdot 32}{\pi D^3 (mm^3)} \tag{3}$$

$$\sigma = \frac{560.51 W}{D^3} \left(\frac{N}{mm^2} \right) \tag{4}$$

Where,
W= Applied load & D= diameter of the specimen on tested section.

A relation developed between equivalent stresses and applied loads for both experimentation and simulation as shown in Fig. 10. The results show smooth relations between loads and equivalent stresses. For a specific load the higher stress in experimentation with respect to simulation represents that there is some notch sensitivity is present in actual environment while in simulation it is considered that the stresses are uniformly distributed on the tested section of the specimen. Due to notch sensitivity it is common practice to multiply the equivalent stresses with stress concentration factor, Kt, resulting into the higher values of stress for corresponding load in experimentation. The stress concentration factor is totally dependent on the geometry of the notch present on the tested section.

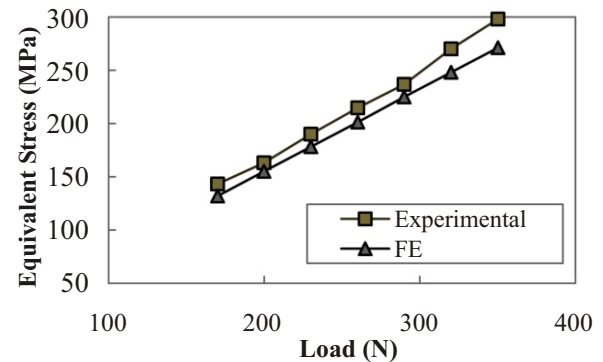


Fig. 10. Comparison of equivalent stress for their specific loads

As the specimens are under combined loadings so due to bending there is deflection observed in the tested specimens. The deflection is calculated by using Eq. 5

$$y_{max} = \frac{ML^2}{8EI} \tag{5}$$

Where, M = Bending moment

The more deflection in experimental work with respect to simulation as shown in Fig. 11 is due to the effect of varying equivalent stresses.

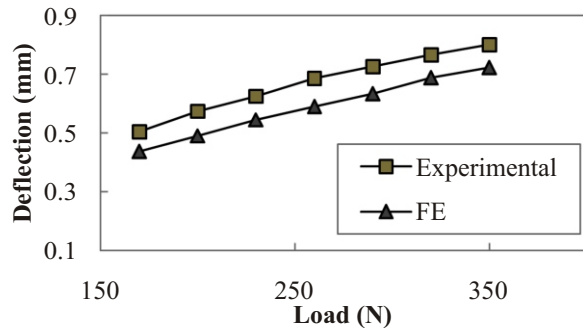


Fig. 11. Comparison of deflections for their specific loads

The prediction of fatigue life is generally made with the help of S-N curve for that specific material. The most important portion of this curve is the 'knee' portion because it defines the endurance limit or fatigue life. Below this portion of the curve the material withstand infinite number of cycles without failures. The S-N of the experimental and simulation data for the subjected material is shown in Fig. 12.

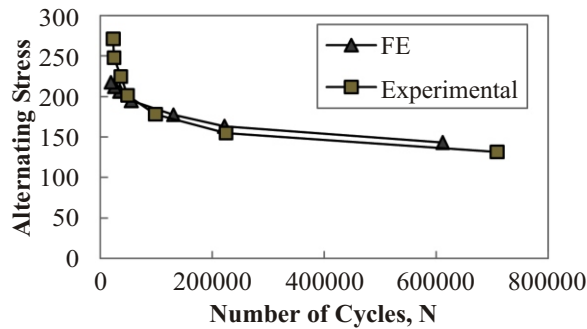


Fig. 12. S-N curves

The knee portion of the both curves is nearly same which represents the verification of the experimental results with the help of numerical simulation. From Fig. 12, it is also represented that both curves becomes nearly parallel to x-axis of the figure after knee point which shows that there is no fatigue failure is taken place regardless of the applying number of cycles or cyclic load.

V. MICROSTRUCTURE

The base metal (BM) is in the form of solid solution type. The strengthening particles of Al_2Cu are randomly scattered in this mechanical mixture of aluminum alloy as shown in Fig. 13. The grains are rolled and of average size. The microstructure of BM is observed after the solution heat treatment when there is

no aging of the metal is taken place at all. However due to non-uniformity of temperature distribution during the heat treatment, some precipitate free zones (PFZ) are also observed in Fig. 13.

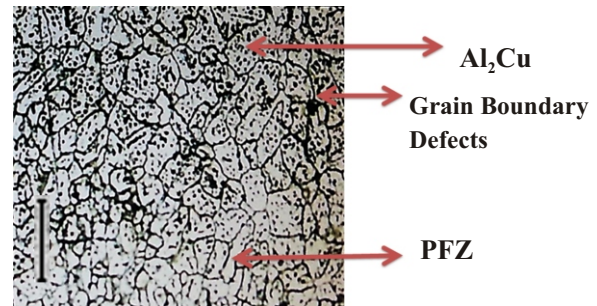


Fig. 13. Microstructure of base metal

These PFZ's are created due to artificial aging of the alloy. At some rare places the grain boundaries defects are also seen due to the crucial thermal or mechanical stresses, applied during preparation of specimens. The zone which is present in between the BM and weld nugget zone (WNZ) is heat affected zone (HAZ). The grain structure of HAZ is small sized and equiaxed as shown in Fig. 14.

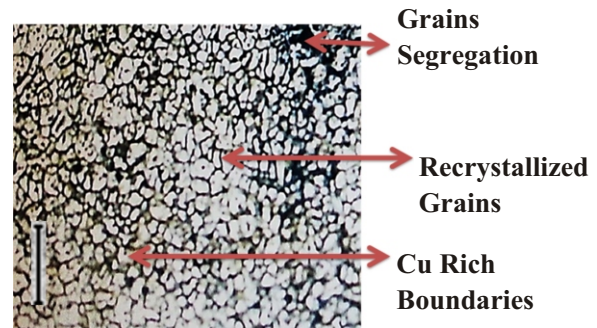


Fig. 14. Microstructure of HAZ

There is somehow recrystallization of grains is taken place. However due to neighboring of WNZ it also experiences very high temperature of welding torch and this causes the migration of strengthening particles towards grain boundaries. Depletion of copper containing particles from grains makes this zone the most fragile one. Some very near portions of HAZ toward WNZ also show the grains detachments due to thermal imbalance. While in WNZ there is molten metal pool is formed during welding. When the sudden cooling of this molten metal is taken place then a dendritic structure is observed under metallurgical microscope as shown in Fig. 15.

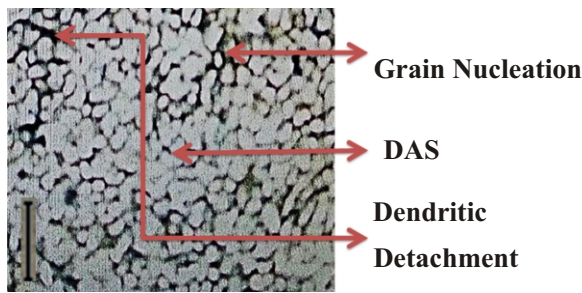


Fig. 15. Microstructure of WNZ

This rapid cooling imparts the brittle properties to the welded parts. When there is improper cooling of the molten pool is happened then the dendrite arm spacing (DAS) is increased very rapidly. The origination of the dendritic structure in WNZ is always started with nucleation at micro level.

VI. CONCLUSION

It is concluded from this research that due to TIG welding of AA2219-T87, using filler alloy of AA2319, different zones are produced. The sudden loss of mechanical properties, hardness & tensile, are observed in HAZ & WNZ with respect to BM. It is tried to estimate the fatigue life of the subjected alloy after TIG weldment by assessing the S-N curves. The effects of stresses due to combined loading (cyclic + bending) are experimentally calculated and verified through numerical simulation. It is also found the relation between the alternating stresses and the failure cycles is $S_a = 1842 \times N^{-0.19}$ for this specific alloy with the specific welding type. A fine distribution of second phase particles (Al_2Cu) due to pre-heat treatment is observed in round and semi elongated grains. Due to cooling rate instability precipitate free zones (PFZs) are also observed in base metal which are responsible for sudden crack propagation. The grain shifting towards boundaries is the prime cause of fragileness of HAZ. The sudden cooling of molten metal pool in WNZ imparts the brittleness properties to weldment.




REFERENCES

[i] J. R. Davis, Aluminum and aluminum alloys. ASM international. 1993.
 [ii] A. Kumar & S. Sundarajan, Optimization of pulsed TIG welding process parameters on mechanical properties of AA 5456 Aluminum alloy weldments. Materials & Design, 30(4),1288-1297, 2009.
 [iii] C. Liljedahl, J. Brouard, O. Zanellato, J. Lin, M. Tan, S. Ganguly, P. E Irving, M. Fitzpatrick, X. Zhang, L. Edwards, Weld residual stress effects on fatigue crack growth behavior of aluminum alloy 2024-T351. International Journal of

Fatigue, 31(6), 1081-1088, 2009.
 [iv] R. E. Little, Tables for estimating median fatigue limits. ASTM, 1981
 [v] H. Mayer, M. Papakyriacou, B. Zettl, S. Vacic, Endurance limit and threshold stress intensity of die cast magnesium and aluminum alloys at elevated temperatures. International journal of fatigue, 27(9), 1076-1088, 2005.
 [vi] Y. H. Zhang, S. J. Maddox, Fatigue life prediction for toe ground welded joints. International Journal of Fatigue, 31(7), 1124-1136, 2009.
 [vii] T. Nykänen, Marquis, T. Björk, "A simplified fatigue assessment method for high quality welded cruciform joints. International Journal of Fatigue, 31(1), 79-87, 2009.
 [viii] M. Shah, C. Mabru, F. Rezai-Aria, Investigation of crack propagation in X38CrMoV5(AISI H11) tool steel at elevated temperatures. Procedia Engineering, 2(1), 2045-2054, 2010
 [ix] M. Shah, M. Ali, A. Sultan, M. Mujahid, H. Mehmood, N. U. Dar, M. Shuaib, An Investigation into the Fatigue Crack Growth Rate of Electron Beam-Welded H13 Tool Steel: Effect of Welding and Post-Weld Heat Treatment. Metallography, Microstructure, and Analysis, 1-12, 2013.
 [x] A. Sultan, R. A. Pasha, M. Ali, M. Z. Khan, M. A. Khan, N. U. Dar, M. Shah, Numerical simulation and experimental verification of CMOD in SENT specimen: Application on FCGR of welded tool steel. Acta Metallurgica Sinica (English Letters), 26(1), 92-96, 2013.
 [xi] A. Norman, V. Drazhner, P. Prangnell, Effect of welding parameters on the solidification microstructure of autogenous TIG welds in an Al-Cu-Mg-Mn alloy. Materials Science and Engineering: A, 259(1), 53-64, 1999.
 [xii] Wang, X. Lu, D. H. Wang, Investigation of surface fatigue micro crack growth behavior of cast Mg-Al alloy. Materials Science and Engineering: A, 364(1), 11-16, 2004.
 [xiii] C. Schweizer, T. Seifert, B. Nieweg, P. Von Hartrott, H. Riedel, Mechanisms and modelling of fatigue crack growth under combined low and high cycle fatigue loading. International Journal of Fatigue, 33(2), 194-202, 2011.
 [xiv] J. K. Donald, Introducing the compliance ratio concept for determining effective stress intensity. International Journal of Fatigue, 19(93), 191-195, 1997.
 [xv] K. Donald, P. C. Paris, An evaluation of ΔK_{eff} estimation procedures on 6061-T6 and 2024-T3 aluminum alloys. International Journal of Fatigue, 21, S47-S57, 1999.
 [xvi] A. G. Gavras, D. A. Lados, J. Keith Donald, A unified method of design for fatigue crack growth resistance in structural materials.

International Journal of Fatigue, 47, 58-70, 2013.
 [xvii] D. A. Lados, D. Apelian, P. E. Jones, J. F. Major, Microstructural mechanisms controlling fatigue crack growth in Al-Si-Mg cast alloys. Materials Science and Engineering: A, 468, 237-245, 2007.
 [xviii] R. Atta-ur-Rahman, M.A. Nasir, M. Ullah et al. Demarcation of Fatigue Crack Cumulative

Damage (Initiation+ stage I) of Aluminum Alloy under Combined Loading. Life Science Journal, vol. 10, no. 12s, 2013.
 [xix] Mudaser ullah, R. Rahman & W. Asghar, Fatigue Life Estimation of Different Welding Zones of Oxy Acetylene Welded Aluminum Alloy (AA 5052-H32). Nucleus, vol. 50, no. 3, 261-265, 2013.

Authorship and Contribution Declaration			
	Author-s Full Name	Contribution to Paper	
1	Mr. Mudaserullah (Main/principal Author)	Proposed topic, basic study Design, methodology and manuscript writing	
2	Prof. Dr. Ghulam Yasin Chohan (2nd Author)	statistical analysis and interpretation of results etc.	
3	Mr. Qasim Ali (3rd Author)	Data collection, Literature review & Referencing	
4	Dr. Muhammad Ali Nasir (4th Author)	Mechanical Testing and Data interpretation, Results & Discussion	